Fully-Propulsive Mars Atmospheric Transit Strategies for High-Mass Payload Missions

ENS Christopher L. Marsh, USN
Georgia Institute of Technology
Atlanta, Georgia 30332-0150
(404) 894-7783
christopher.l.marsh@gatech.edu

Robert D. Braun
Georgia Institute of Technology
Atlanta, GA 30332-0150
(404) 385-6171
robert.braun@ae.gatech.edu

Abstract—A systems analysis focused on the use of propulsion during entry, descent, and landing at Mars is presented. The propellant mass fractions of various fully-propulsive EDL strategies are presented. A key aspect of the study is the propellant costs of meeting specified heat rate constraints and the trade between TPS mass and technology requirements vs those for propulsive deceleration. Propulsive strategies considered include a constant-thrust gravity turn as well as variable-thrust trajectory designs. A control law for heat rate constrained trajectories is provided. Sensitivity to the vehicle's propulsive capabilities is explored. A comparison is presented between the fully-propulsive EDL architecture and EDL systems in which significant aeroassist technology is employed. With this information, an overview of the impact of a fully-propulsive EDL system on spacecraft design and functionality is offered.[1] [2]

TABLE OF CONTENTS

1. INTRODUCTION

The United States has safely landed six spacecraft on Mars starting with Viking 1 and 2 in 1976 and continuing to the recently landed Phoenix. However, the largest landed mass of these missions is 590 kg [1]. While NASA is currently preparing for flight of the Mars Science Laboratory and its 900 kg landed payload [2], the Vision for Space Exploration calls for eventually sending humans to Mars with landed masses in range of 40 to 80 metric tons [3]. One of the most significant challenges of a human Mars mission is in the area of entry, descent, and landing (EDL). Due to the presence of a thin but significant atmosphere at Mars, current Mars EDL strategies and technologies depend heavily on aerodynamic forces to slow the vehicle. These concepts are largely derived from Viking and Earth-return experience. However, this proven technology does not allow for extension of landed mass capability to the level required for human exploration [1]. As an example, NASA's previous Design Reference Mission [4] required a cluster of three 50-m diameter Viking heritage parachutes to be deployed supersonically. This requirement is likely well beyond the supersonic disk-gap-band parachute capability.

Due to the low density of the Mars atmosphere (approximately $1/100^{th}$ as dense as Earth's), a Mars landing architecture comparable to that used in human exploration of the Moon is a natural consideration. In the Apollo program, propulsion was employed in the descent and landing sequence, where the lunar landers' propulsion system provided all of the ΔV required from lunar orbit to landing. Although not the main contributor in the EDL system, propulsion has been used in several robotic missions to Mars. A summary of the use of propulsion in the lunar and Mars landings is given in Table 1 [1],[5-15]. The capabilities required by human Mars exploration greatly surpass those outlined in Table 1.

This paper investigates the ability to employ a fully-propulsive atmospheric transit strategy at Mars for high-mass payload missions. The objective of this systems analysis effort is to provide a fully-propulsive reference architecture for comparison with EDL architectures that employ aeroassist technology. In this study, fully-propulsive descent refers to deceleration sequences that do not include aeroassist technology elements such as lifting aeroshell configurations, an ablative thermal protection system, parachutes, or inflatable aerodynamic decelerators (IAD). Instead, these architectures consist of powered flight from Mars orbit or hyperbolic approach conditions to the surface in which deceleration is achieved through a combination of propulsive thrust and aerodynamic drag. The study explores the potential of avoiding heating and g-load constraints by altering the vehicle's deceleration. Propulsive strategies considered include a constant-thrust gravity turn as well as variable-thrust trajectory designs. In addition, the use of a fully-propulsive descent system is shown to allow for landing site divert options throughout the entry, descent, and landing sequence. This study examines the system requirements and extent of these propulsive capabilities.

1

[1] 978-1-4244-2622-5/09/$25.00 ©2009 IEEE.

[2] IEEEAC paper#1219, Final Version, Updated 2009:01:09

Table 1 - Historic Uses of Propulsion in EDL [1],[5-15]

	Apollo	Viking 1/2	MPF	MER-A/B	Phoenix	MSL
Use of propulsion	lunar deorbit and landing	terminal descent	terminal descent and flyaway	terminal descent and flyaway	terminal descent	terminal descent and flyaway
Propellant type	N_2O_4/A-50	hydrazine	solid rockets	solid rockets	hydrazine	hydrazine
ΔV imparted, m/s	2010	220	63	57.4/61.8	55.3	120
Maximum thrust, kN	43.9	8.0	23.8	23.3	30.3	24
Throttling	10 - 60% of T_{max}	10:1	none	none	off-pulsed	13 - 100% of T_{max}
$I_{sp,}$ sec	311	210	260	273.9	212.5	210
Mass of propellant, kg	8165	185	20.7	27.1	37.4	340
Total mass of engines, kg	113	23	30.7	17.5	30	72
Landed mass, kg	7000-8250	590	360	539	382	900

2. APPROACH

Simulation

To perform the necessary studies, a MATLAB-based entry simulation was created to propagate the three degree-of-freedom translational equations of motion from a given set of initial conditions until termination at the surface of the planet. The simulation models a spherical, rotating planet with forces due to gravity, thrust, and drag. The vehicle follows a ballistic trajectory and does not take advantage of aerodynamic lift. The vehicle used in the study is a 70° sphere-cone similar to that used by the robotic missions referenced in Table 1. The simulation uses a tabulated coefficient of drag as a function of Mach number and interpolates between data points. The reference atmosphere used is tabulated from the Mars Pathfinder mission.

Simulation validation is critical to ensure the accuracy of the results of this study. To do so, a Mars Pathfinder simulation was compared against a trajectory of the same mission simulated with the Program to Optimize Simulated Trajectories (POST) [16]. As shown in Figure 1 and Table 2, the trajectory generated by the MATLAB entry simulation is in excellent agreement with the POST trajectory. Position, velocity, flight path angle (FPA), dynamic pressure, heating, and g-load calculations were validated through this process.

Table 2 – Event Comparison for Trajectory Validation

Event	This Study	POST	Difference (%)
Entry			
Time (sec)	0	0	0.00
Altitude (m)	128000	128000	0.00
Relative Vel. (m/sec)	7479	7479	-0.01
Relative FPA (º)	-13.65	-13.65	0.00
Parachute Deploy			
Time (sec)	154.5	154.5	0.00
Altitude (m)	9916	9916	0.00
Relative Vel. (m/sec)	414.5	414.5	0.01
Relative FPA (º)	-23.35	-23.35	-0.01
Dyn. Pressure (Pa)	585.0	585.0	0.00
Heatshield Jettison			
Time (sec)	174.5	174.5	0.00
Altitude (m)	8217	8219	-0.03
Relative Vel. (m/sec)	90.36	90.23	0.14
Relative FPA (º)	-47.29	-47.33	-0.08
Dyn. Pressure (Pa)	32.07	31.98	0.30
Trajectory Termination			
Time (sec)	359.8	359.8	0.01
Altitude (m)	-2408	-2408	0.00
Relative Vel. (m/sec)	42.64	42.64	0.01
Relative FPA (º)	-89.88	-89.88	0.00
Dyn. Pressure (Pa)	21.55	21.55	-0.02

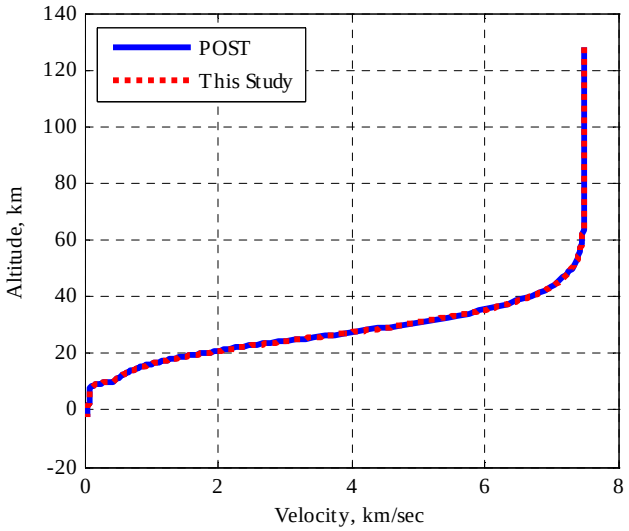

Figure 1 - Trajectory Validation

The simulator has the ability to use various thrust control modules. These modules specify the thrust direction and magnitude throughout the trajectory. The thrust control module and the mass impact of the use of thrust were validated against an independent simulation used in a recent assessment of Mars pinpoint landing performance [17]. A Newton-based solver is used within the simulator to calculate the altitude at which to begin the constant-thrust gravity turn as to ensure a velocity of less than 0.1 m/sec at landing. Figure 2 and Table 3 show the excellent agreement between trajectory parameters for the constant-thrust gravity turn validation case.

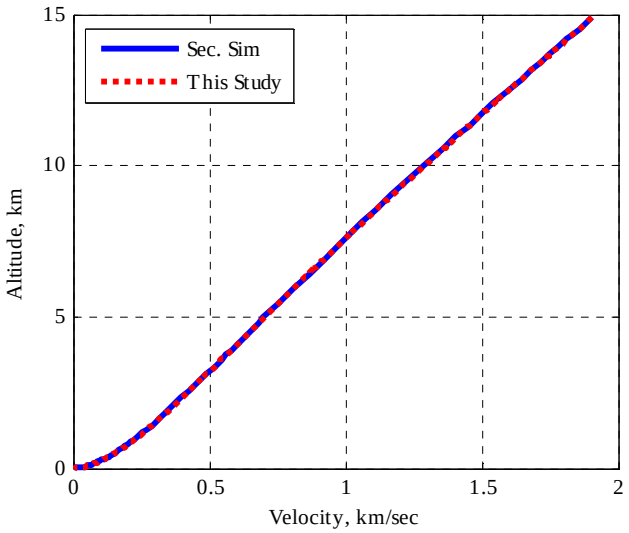

Figure 2 - Propulsive Maneuver Validation [17]

Table 3 - Event Comparison for Propulsive Maneuver Validation

Event	This Study	Secondary Simulator [17]	Difference
Ignition			
Time (sec)	0.00	0.00	0.00
Mass (kg)	9713.24	9713.24	0.00
Altitude (m)	14885.40	14885.40	0.00
Relative Vel. (m/sec)	1902.73	1902.73	0.00
Relative FPA (º)	-6.38	-6.38	0.00
Trajectory Termination			
Time (sec)	95.36	95.36	0.00
Mass (kg)	6615.61	6615.71	0.10
Altitude (m)	0.00	0.17	0.17
Relative Vel. (m/sec)	0.07	0.10	0.03
Relative FPA (º)	-82.36	-81.41	0.95

Modeling

Throughout the study, vehicle performance is based largely on the ability to deliver payload to the Mars surface. Therefore, modeling the vehicle's mass is a crucial aspect of the study. The vehicle's initial mass is broken into five general categories: propulsion system, thermal protection system (TPS), structure, auxiliary systems, and payload. A majority of the mass model is based on the work of Christian, et al. [18] such that a comparison to recent aeroassist technology studies can be performed.

Propulsion System—The main component of the propulsion system mass is the propellant required for descent and landing. This value is calculated throughout the simulation as a part of the vehicle state as shown in Equation 1. Since there are no mass drops during the fully-propulsive descents provided in this study, the propellant required by a specific trajectory is calculated by subtracting the landed mass from the vehicle's initial mass.

$$\dot{m} = T / I_{sp} g_0 \qquad (1)$$

In systems level studies, I_{sp} is generally determined through the type of fuel used. As in most previous human Mars exploration studies, the reference propellant assumed is LOX/CH_4. This choice is based largely on the ability to produce methane while on the surface of Mars and the need for commonality in the Earth-Mars and Mars-Earth transportation systems required for human exploration [4],[18]. The reference case of this study assumes an I_{sp} of 350 sec, although the mass fraction sensitivity to I_{sp} is also provided. The vehicle's thrust, T in Equation 1, is assigned by the controller and is limited in magnitude by a specified thrust to weight ratio (T/W).

In the reference case, a constant-thrust gravity turn is used for the terminal segment of the EDL sequence. Gravity turns of the same ΔV require less fuel for increasing thrust levels. Theoretically, gravity turns are most efficient if employed with infinite thrust at the instant before touchdown. Figure 3 shows that a mass savings of more than 15% can be realized if full throttle is used instead of a throttle setting of 50% for a vehicle with the capability of producing a thrust of 670 kN.

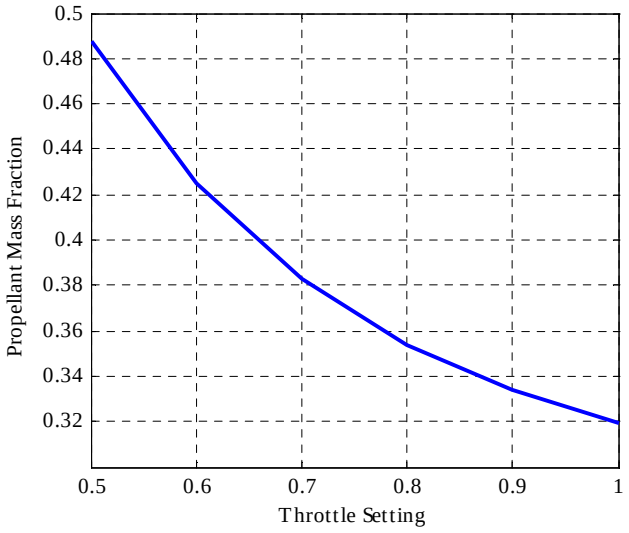

Figure 3 - Propellant Mass Fraction of a Terminal Gravity Turn Performed at Various Throttle Settings for a 60 mT, 10 m Diameter Vehicle

As such, in this investigation, the terminal gravity turn maneuvers utilize the maximum allowable thrust set by a wet vehicle thrust to weight ratio. The assigned thrust to weight ratio is based on the initial weight of the vehicle at Mars. The thrust is determined through this manner so that engine capability is scaled with the size of the vehicle. Previous studies have used T/W ratios ranging from 2 to 5 [18]. The reference case in this study uses a T/W of 3. The sensitivity to this parameter is explored later.

In modeling the mass of the engines, it is necessary to specify the quantity of engines required and the mass of each engine. Individual engines are scaled according to the following relationship:

$$m_{engine} = 0.00144T + 49.6 \qquad (2)$$

where T is the engine thrust in N and m_{engine} is the engine mass in kg. The relationship was developed by Christian, et al. through regression analysis of data for conceptual LOX/CH_4 engines [18]. The upper bound of the thrust of the engines used in forming the relationship was 200 kN [19]. In determining the mass of the engines for the current study, the thrust produced by a single engine is limited to this value. Limiting the maximum thrust that a single engine can produce and specifying the required total thrust of the propulsion system dictates the minimum number of engines on the vehicle. However, more consideration of the number and placement of engines is necessary.

It has been shown that individual engines placed in the center of the body can effectively eliminate the drag of the vehicle; whereas, placing engines at the periphery of the vehicle can preserve the vehicle's aerodynamic drag for thrust coefficients lower than one [20]. The mass savings of conserving the vehicle's drag profile during thrusting maneuvers (as much as a 25% advantage) is shown in Figure 4. In this investigation, the reference case assumes that the drag of the vehicle is fully conserved during propulsive maneuvers.

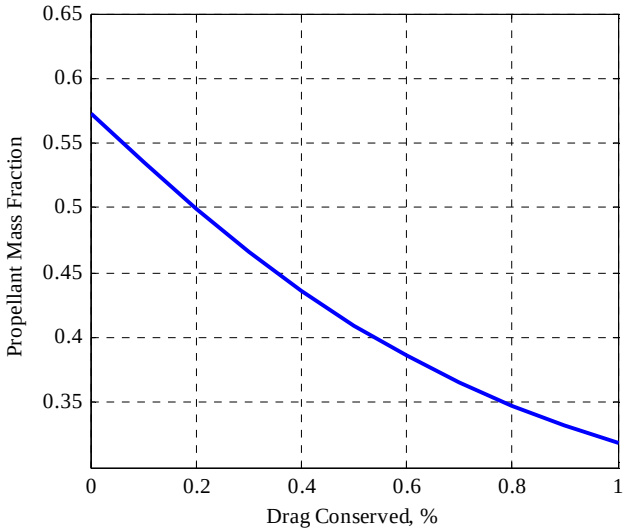

Figure 4 - Effect of Conserving Aerodynamic Drag During Propulsive Maneuvers for a 60 mT, 10 m Diameter Vehicle

Assuming sufficient throttling authority, additional engines also allow for engine-out capabilities thus increasing the system reliability. For these reasons, the vehicles in this study have no less than four engines situated on the periphery of the vehicle's body.

Propellant tanks also need to be considered in the vehicle modeling. For this study, the propellant tanks are sized according to the volume of propellant needed for the trajectory. An oxidizer to fuel ratio of 3.5 is assumed with the density of the methane and liquid oxygen to be 422.6 kg/m^3 and 1140.1 kg/m^3 respectively. The tanks are assumed to be made of titanium with an operating pressure of 1.4 MPa. These parameters are consistent with those used by Christian, et al. [18],[21].

Structure—Using historical and conceptual crewed vehicles as data points, Christian, et al. conservatively estimated the structural mass fraction of the entry capsule as 25% of the vehicle's dry mass. For comparison purposes, this same assumption is made in the current study.

Thermal Protection System—During atmospheric entry, radiative and convective heating of the vehicle are of concern. At Mars, significant radiative heating can be encountered at velocities greater than 6 km/sec. However, radiative heating becomes negligible at velocities less than 6 km/sec [22]. All velocities experienced in this study are below 6 km/sec, and therefore, radiative heating is neglected. Stagnation-point convective heating is calculated using Equation 3.

$$\dot{q}_{conv} = k\sqrt{\rho / r_n} \cdot v_{rel}^3 \tag{3}$$

In Equation 3, r_n is the nose radius of the vehicle and is approximated as a quarter of the vehicle's diameter for this study. The constant, k, depends on the composition of the Martian atmosphere and is 1.9027 x 10^{-8} $kg^{1/2}/cm^2$ for the convective heat rate to be computed in W/cm^2.

Vehicle heating is generally mitigated with the use of an ablative TPS. For cases which require TPS, a low fidelity estimation of the TPS mass is used. The TPS mass estimation is based on the total heat load and is provided in Equation 4 [23].

$$MF_{TPS} = 0.091\left(q_{conv,total}\right)^{0.51575} \tag{4}$$

This study explores the possibility of eliminating the entry system TPS by flying a heat-rate constrained trajectory. Without an ablative thermal protection system, an upper bound must be placed on the heat rate to limit the thermal stresses placed on the vehicle. Assuming the system is in equilibrium, the heat rate limit can be computed for a given structural material.

$$\dot{q}_{conv} = k\varepsilon T^4 \tag{5}$$

In Equation 5, T is the highest acceptable temperature of the vehicle's forebody material in Kelvin, k is the Stefan-Boltzmann constant (5.67 x 10^{-8} W/m^2K^4) and, ε is the emissivity of the spacecraft material.

Auxiliary Systems—The spacecraft will include several other components that for simplicity have been combined into a category referred to as auxiliary systems. This includes but is not limited to command, control, and communications, power, and life support systems. Mass sizing of the auxiliary systems is conducted in the same manner as done by Christian, et al. [18].

Margin—Due to uncertainties in the mass models, 15% of the vehicle's dry mass is allocated to margin. This margin approach remains consistent with the work of Christian, et al. [18].

Payload—Applying the above definitions, the payload of the spacecraft is defined as the mass remaining once the above system masses are subtracted from the vehicle's landed mass.

$$\begin{aligned} m_{payload} = m_{landed} - m_{prop\ sys} - m_{structure} \\ - m_{TPS} - m_{aux\ sys} - m_{margin} \end{aligned} \tag{6}$$

Reference Mission

The current study considers two entry options: direct entry from a hyperbolic approach trajectory and entry from orbit. In the direct entry case, the simulation is initiated at a 400 km altitude with an inertial velocity of 5.85 km/sec, a state that is equivalent to 6 km/sec at atmospheric interface (altitude of 125 km). The initial flight path angle of the vehicle is optimized with respect to the mission's overall propellant mass fraction (PMF). In the entry from orbit cases, the vehicle is initially assumed to be in a 400 km altitude circular orbit (inertial velocity of 3.36 km/sec). The vehicle performs a deorbit maneuver to change its velocity and flight path angle. Once again, the magnitude of the deorbit burn is optimized with respect to overall PMF. Once the spacecraft has begun its descent sequence, there are no deployments, separations, or changes in configuration. The vehicle follows a ballistic trajectory, relying only on propulsion and drag for deceleration. All trajectories end with a constant-thrust gravity turn that is performed at maximum thrust and initiated at a time consistent with the vehicle T/W. The reference trajectory deceleration is performed through only aerodynamic drag and this terminal gravity turn maneuver.

Throughout the EDL sequence, there are various constraints that must be satisfied. First, the landing conditions must be met. A Newton-based solver is used to calculate the altitude of the initiation of the terminal deceleration phase. During terminal descent, the constant-thrust gravity turn is employed to arrive at the targeted surface elevation within 1 m and at less than 0.01 m/sec. In the reference trajectory, no additional ΔV is provided for a constant velocity, vertical descent segment or divert maneuver that may ultimately be required. A maximum g-limit constraint is also placed on the trajectories. Due to an expected astronaut deconditioning period on the order of 6 to 9 months, the maximum g-load constraint is set to 5 Earth g's. A heat rate constraint is also placed on the trajectories to determine if the ablative thermal protection system employed by current robotic missions can be eliminated through the use of propulsion early in the trajectory. The g-limit and heat rate constraints are not implemented in the reference trajectories but are used later in this study.

3. RESULTS

Reference Trajectories

As a benchmark for this investigation, a reference trajectory for both the direct entry and entry-from-orbit scenarios is first established. The vehicle used for these reference cases is described in Table 4. The provided mass, ballistic coefficient, and T/W are for the vehicle at the initiation of the from-orbit or direct descents. Note that in these reference cases, deceleration is accomplished without aeroassist technology elements such as lifting configurations, parachutes, or inflatable aerodynamic decelerators.

Table 4 - Baseline Vehicle Parameters

Baseline Vehicle	
Initial mass, mT	60
Vehicle diameter, m	10
Ballistic coefficient, kg/m^2	477.5
Initial T/W	3
$I_{sp,}$ sec	350

The entry-from-orbit reference case uses the mass-optimum deorbit ΔV, while the direct entry reference case begins with the mass-optimum initial flight path angle. At the end of each of these trajectories, a constant-thrust terminal gravity turn is used to ensure a safe landing. For the majority of the descent, the vehicle is not under power. For the entry-from–orbit reference case, propulsion is used for the deorbit maneuver and the gravity turn segment. For the direct entry reference case, propulsion is only used for the gravity turn segment. The reference trajectories are outlined in Figure 5 and Table 5.

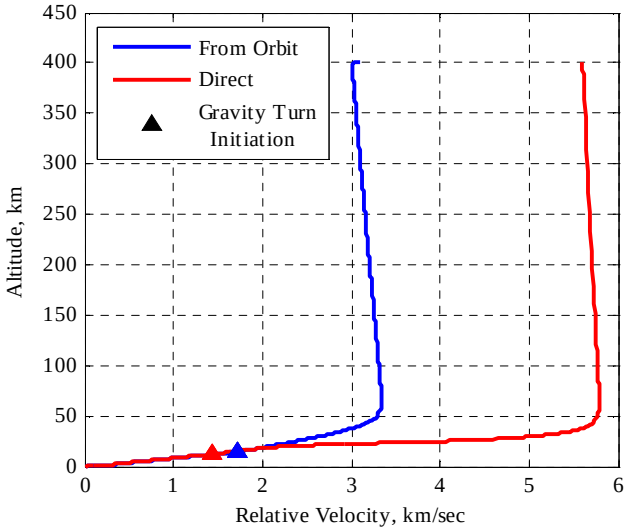

Figure 5 - Reference Trajectories

Table 5 - Events and Parameters of the Reference Trajectories

Event	From Orbit	Direct
Simulation Initiation		
Time (s)	-2256.75	-166.90
Altitude (m)	400000.00	400000.00
Relative Vel. (m/s)	3090.80	5600.91
Relative FPA (°)	0.00	-22.02
Entry Interface		
Time (s)	0.00	0.00
Altitude (m)	125000.00	125000.00
Relative Vel. (m/s)	3283.84	5755.36
Relative FPA (°)	-2.68	-11.56
Gravity Turn Initiation		
Time (s)	918.16	319.32
Altitude (m)	14282.82	11702.12
Relative Vel. (m/s)	1711.13	1436.74
Relative FPA (°)	-7.37	-6.98
Trajectory Termination		
Time (s)	1008.62	404.31
Altitude (m)	-0.01	-0.01
Relative Vel. (m/s)	0.00	0.00
Relative FPA (°)	-87.90	-88.49
Parameter		
PMF (%)	31.85	27.61
Peak Heat Rate (W/cm^2)	7.12	49.85
Total Heat Load (J/cm^2)	2373.77	5697.99
Peak g-Load (Earth g's)	2.65	3.10
Peak Dyn. Pressure (Pa)	6780.03	14446.97

No in-flight constraints are considered in these two reference cases. Therefore, the mass optimization finds an initial state of the vehicle which maximizes drag throughout the trajectory. This strategy minimizes the ΔV required by the terminal gravity turn. Clearly, an increase in drag results in an increase in heating. This issue is discussed later in this section.

To investigate the consequences of changing the arrival mass, the reference EDL sequences are computed for arrival masses ranging from 20 to 100 mT. The initial FPA or deorbit ΔV is optimized for each case. The results are given in Figure 6. The propellant mass fraction significantly increases with an increase in initial mass for both entry scenarios. For the baseline I_{sp} of 350 sec, the PMF increases approximately 10% for each doubling of arrival mass.

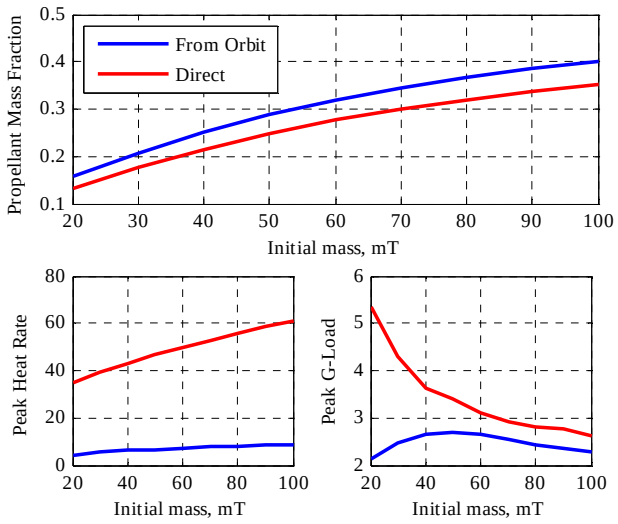

Figure 6 - PMF, Peak Heat Rate, and Peak G-Loads for 10 m Diameter Vehicle

Note that the higher energy cases (direct entry) require less propellant than the corresponding cases originating in orbit. The majority of this difference is found in the requirement for a deorbit burn in the entry-from-orbit cases. For the baseline vehicle, the deorbit burn costs 1.48 mT (2.5% of the initial mass) leaving a 1.75% of PMF difference between the two cases. Further examination of the baseline vehicle's reference trajectories reveals the source of the difference. Due to a higher velocity, the direct entry trajectory experiences approximately 2.55 km/sec more ΔV due to drag. The difference in drag-induced ΔV is greater than the difference in initial velocities by 55 m/sec. Using the ideal rocket equation, this drag benefit converts to a 1.6% propellant mass fraction savings, accounting for the majority of the difference highlighted earlier. However, with the increased drag, the peak heat rate increases over 40 W/cm^2 between the entry-from-orbit and direct entry cases for the baseline vehicle. As shown in Figure 6, these trends continue for increasing initial masses resulting in larger differences in PMF at the cost of even larger increases in the peak heat rate.

Addition of a Heat Rate Constraint

Assuming the primary structure and forebody is constructed of steel, the vehicle's strength drastically decreases for temperatures exceeding 300°C [24]. If the vehicle is in thermal equilibrium and assuming that the steel used has an emissivity of 0.8, a stagnation-point temperature of 300°C corresponds to a convective heat rate of approximately 0.5 W/cm^2 according to Equation 5. As shown in Figure 6, a vehicle made primarily of steel would require some form of TPS if it followed the reference trajectory.

In an attempt to eliminate the need for TPS, a heat rate constraint is placed on the vehicle's trajectory. To meet this constraint, a mid-trajectory propulsive segment is included in the EDL sequence. This added maneuver increases the vehicle's propellant mass fraction. However, by slowing the vehicle at the right point in the trajectory, the peak heat rate can be reduced. Therefore, it may be possible to reduce, or even eliminate, the mass, complexity, and cost of an ablative TPS.

The mid-trajectory propulsive maneuver was first designed as a constant-thrust burn. As with a gravity turn, the thrust was directed in the opposite direction of the velocity. The altitude at which the mid-trajectory burn was initiated, the burn ΔV, and the thrust magnitude of the burn were optimized with respect to landed mass. This burn was performed at constant thrust, but unlike the gravity turn, it was not necessarily performed at maximum thrust. Reducing the thrust magnitude of the mid-trajectory burn allowed for longer burn times thus controlling the vehicle's velocity over an extended period. This proved necessary to meet lower peak heat rate constraints. The propellant mass fractions that result across a range of heat rate constraints for the cases descending from orbit are provided in Figure 7. Since the peak heat rate experienced by the reference trajectory is 7.12 W/cm^2, heat rate constraints greater than 7.12 W/cm^2 have no impact on the PMF as the vehicle flies the reference trajectory with no mid-trajectory burn. Note that for the baseline vehicle (60 mT) entering from orbit, the reference trajectory requires a PMF of 31.9% and Ref [18] estimates a TPS mass fraction of 12.1%. Therefore, the cost of meeting the 0.5 W/cm^2 heat rate constraint is a 16% increase in the PMF.

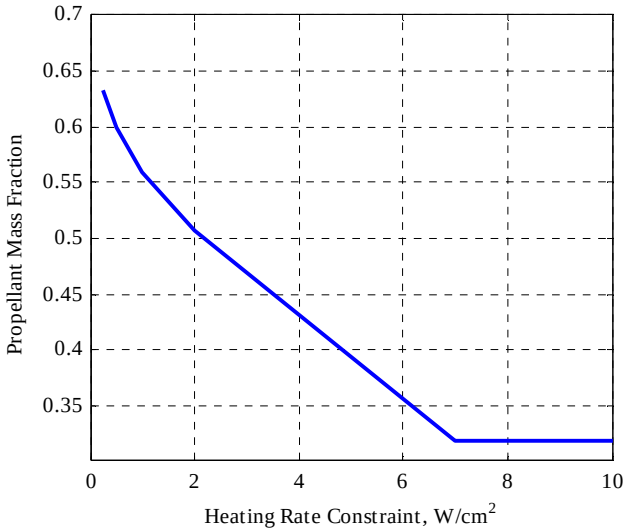

Figure 7 – Propellant Mass Fraction of Baseline Vehicle Descending from Orbit on Heat Rate-Limited Trajectories

Mid-Trajectory Burns with Variable Thrust

The mid-trajectory burn acts to slow the vehicle before the heating constraint is breached. Not only does this maneuver require propellant, but the decrease in velocity also greatly reduces the deceleration due to drag. However, the more mass-optimal trajectories are those that are able to stay on or

near the heating constraint as long as possible, resulting in maximum allowable drag losses. These trajectories also require shorter burns and therefore have lower gravity losses. While experiencing higher integrated heat loads, these trajectories deliver the most payload to the surface. Figure 8 shows that the more mass optimal trajectory is able to maintain its proximity to the heating constraint for a longer period of time, suggesting the need for a variable thrust (throttling) method for the mid-trajectory burn.

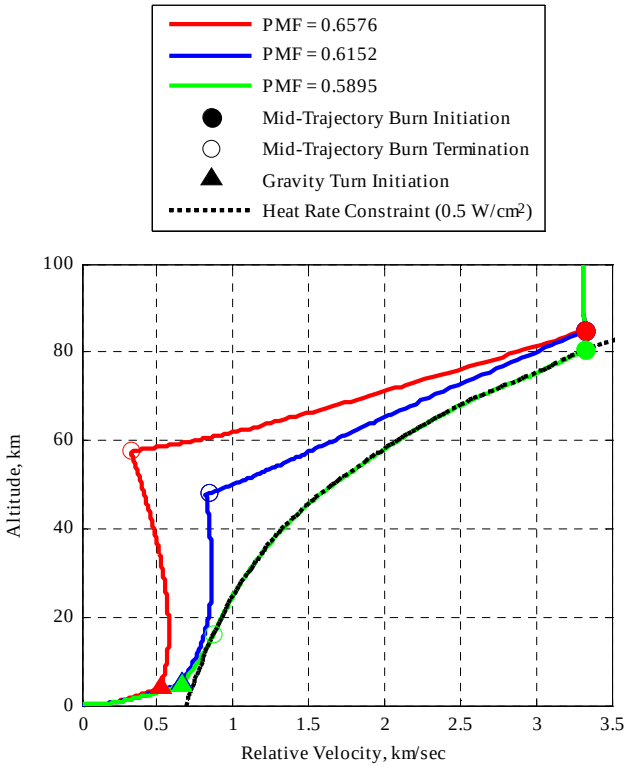

Figure 8 - Trajectories with Respect to the Heat Rate Constraint for the Baseline Vehicle Descending from Orbit

Assuming knowledge of the vehicle's altitude at all times during the trajectory and an accurate density model of the Mars atmosphere, the desired velocity of the spacecraft during the mid-trajectory burn can be calculated by re-arranging Equation 3 into the form shown in Equation 7. As such, defining the heat rate constraint defines the state of the vehicle in this trajectory segment.

$$v_{rel,con} = \left(\frac{\dot{q}_{conv} \sqrt{r_n / \rho}}{k} \right)^{1/3} \tag{7}$$

Assuming that the thrust and drag forces dominate during propulsive maneuvers, the time derivative of the spacecraft velocity can be estimated through Equation 8 where T and D are the thrust and drag forces.

$$\frac{d\vec{v}_{rel}}{dt} = \frac{\vec{T} + \vec{D}}{m} \tag{8}$$

During the mid-trajectory burn maneuver, thrust and drag are directed in the opposite direction of the velocity vector, allowing for a simplification of the thrust and drag vectors in Equation 8. Through discretization, Equation 9 can be formulated from Equation 8.

$$\Delta\vec{v}_{rel} = -\Delta t \frac{T + D}{m} \hat{v}_{rel} \tag{9}$$

In Equation 9, Δv_{rel} is defined as the difference between the actual relative velocity and the desired relative velocity with respect to the heat rate constraint. Δv_{rel} can be thought of as the necessary change in velocity to meet the heating constraint.

$$\Delta\vec{v}_{rel} = \vec{v}_{rel} - \vec{v}_{rel,con} \tag{10}$$

Substituting into Equation 9 and solving for thrust gives the following control law.

$$T = -\left(\frac{m\left(v_{rel} - v_{rel,con}\right)}{\Delta t} - D \right) \hat{v}_{rel} \tag{11}$$

Due to its dependence on information from the previous time step, the controller described above lags the system; the thrust calculated is that necessary to correct the velocity of the previous time step. However, with a sufficiently small time step, the lag of the controller is negligible and the spacecraft closely follows the contour provided by the heat rate constraint. By riding the heat rate contour, the trajectory maximizes velocity losses due to drag without breaching the assumed thermal limits of the spacecraft.

With the variable-thrust control law, the direct entry and entry from orbit reference trajectories are re-simulated. Again, steel is assumed as the primary material of the spacecraft which limits the peak heat rate to 0.5 W/cm^2. As shown in Figure 9 and Table 6, both trajectories ride the heat rate constraint for a considerable portion of the descent. When mass sizing is performed on the direct entry case, a negative payload is calculated as a result of the large PMF (nearly 77%), and the case is deemed infeasible.

While the entry-from-orbit case is able to begin the mid-trajectory burn when the vehicle reaches the heat rate constraint, the direct entry must begin the burn exo-atmospherically. Due to the increased velocity of the direct entry, the vehicle would reach the heat rate constraint along

a much flatter region of the constraint. As the constraint becomes more horizontal (i.e. at higher velocities), a near-hover maneuver is needed to avoid violating the constraint. This points towards increasing the thrust or thrusting primarily in the vertical direction. However, for this study, the thrust magnitude is initially limited by a specified T/W and later, as the vehicle loses mass, by the g-loading constraint. Also, the direction of thrust is always defined in the opposite direction of the vehicle's velocity. The remaining option for meeting the heat rate constraint for high velocity cases is starting the mid-trajectory burn earlier in the trajectory. This allows for decreases in velocity before reaching denser regions of the atmosphere where sufficient heating occurs. The portion of the mid-trajectory burn executed prior to reaching the heat rate constraint is performed at maximum thrust to limit losses. Within the simulation, the altitude at which to begin this burn is explicitly calculated so that the resulting vehicle trajectory is tangent to the heat rate constraint when the two intersect. At this point, the thrust is throttled according to the control law provided by Equation 11. After some time riding the heat rate constraint, drag provides enough deceleration so that thrust is no longer required to meet the constraint. This results in a period of no thrust between the mid-trajectory burn and the final gravity turn maneuver. However, as shown in Table 6, for the case of a 0.5 W/cm^2 constraint, this non-thrusting phase of flight spans a relatively small range of altitudes. These behaviors are shown in Figures 9 and 10.

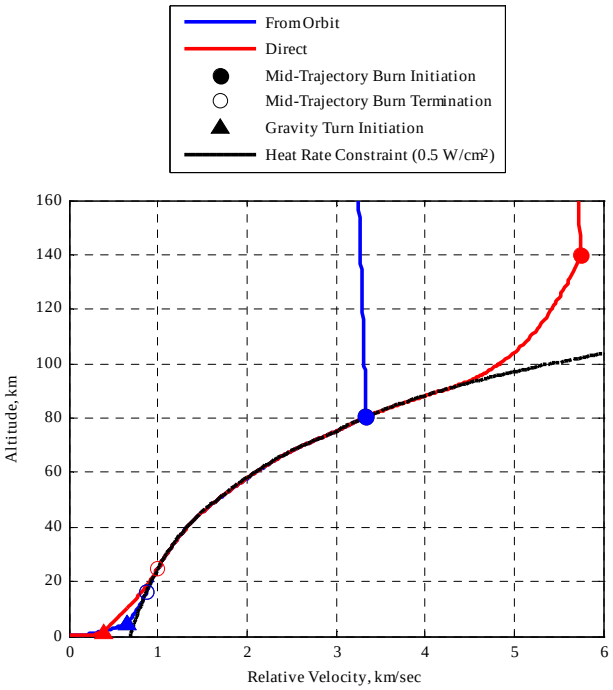

Figure 9 - Mid-Trajectory Burn of the Baseline Vehicle

Table 6 - Events and Parameters of Trajectories Employing Mid-Trajectory Burns

Event	From Orbit	Direct
Simulation Initiation		
Time (s)	-2549.03	-208.99
Altitude (m)	400000.00	400000.00
Relative Vel. (m/s)	3090.80	5597.64
Relative FPA (º)	0.00	-19.96
Entry Interface		
Time (s)	0.00	0.00
Altitude (m)	125000.00	125000.00
Relative Vel. (m/s)	3294.02	5519.16
Relative FPA (º)	-1.88	-6.72
Mid-Traj. Burn Initiation		
Time (s)	700.63	-20.21
Altitude (m)	80562.80	139595.95
Relative Vel. (m/s)	3337.70	5743.48
Relative FPA (º)	-0.23	-8.02
Mid-Traj. Burn Termination		
Time (s)	1404.86	570.98
Altitude (m)	16093.09	24570.61
Relative Vel. (m/s)	871.65	997.06
Relative FPA (º)	-24.21	-19.68
Gravity Turn Initiation		
Time (s)	1437.27	646.73
Altitude (m)	4523.08	1088.87
Relative Vel. (m/s)	657.69	386.61
Relative FPA (º)	-31.43	-39.79
Trajectory Termination		
Time (s)	1462.60	655.32
Altitude (m)	0.44	0.02
Relative Vel. (m/s)	0.00	0.00
Relative FPA (º)	-81.90	-71.69
Parameter		
PMF (%)	58.78	76.65
Peak Heat Rate (W/cm^2)	0.50	0.50
Total Heat Load (J/cm^2)	519.13	290.75
Peak g-Load (Earth g's)	3.31	5.00
Peak Dyn. Pressure (Pa)	2330.78	1387.11

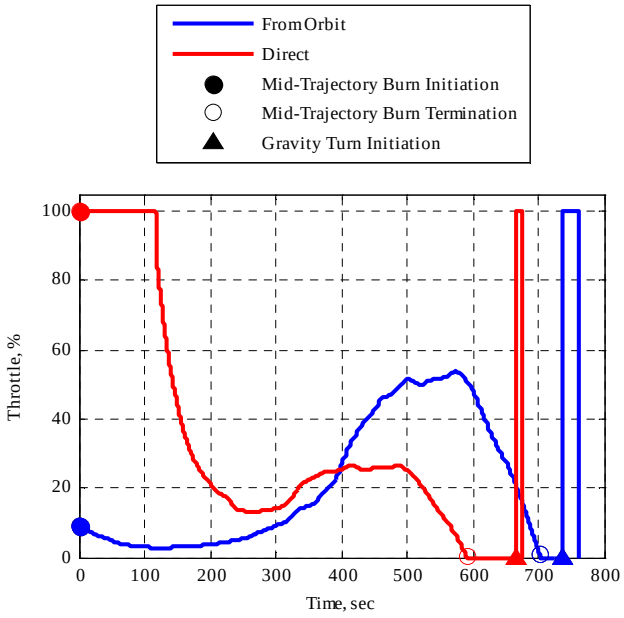

Figure 10 - Control History of Mid-Trajectory and Terminal Propulsive Maneuvers

Propulsion System Performance

To investigate the sensitivity of payload mass to propulsive system performance, the vehicle's thrust to weight ratio and specific impulse are varied. Contrary to the results shown in Figure 3, the vehicle's thrust to weight ratio has negligible impact on the overall propellant mass fraction for heat-rate limited entries, since the mid-trajectory burn is not generally performed at maximum thrust. In the trajectories computed, the mid-trajectory burn ΔV is approximately three times as large as the terminal gravity turn ΔV. Therefore the benefit of having a larger maximum thrust available is not realized. However, bounds can be set on the required thrust to weight ratio based on the heat rate and g-load constraints.

The heat rate constraint defines the lower boundary of the thrust to weight ratio. In the current control structure, the vehicle must have the ability to travel along the heat rate constraint for a significant portion of the trajectory. On an altitude/velocity plot, more thrust is required as the constraint becomes horizontal. For the constraints and trajectories seen in this study, the lower bound on the required T/W is approximately 2.5. For lower thrust to weight ratios, the mid-trajectory burn must be started earlier in the trajectory. With this change, the vehicle reaches a more vertical (less demanding) section of the heat rate constraint. However, starting the mid-trajectory burn earlier has a significant negative impact on the propellant mass fraction.

The upper bound of the vehicle's thrust to weight is determined by the allowable g-load constraint. For 5 Earth g's, the maximum Mars thrust to weight ratio can be calculated as approximately 13. However, due to additional deceleration due to drag (maximum of 1.5 g's for the cases examined in this study), use of this value of maximum thrust during descent would breach the g-loads constraint. As such, a maximum thrust to weight ratio on the order of 9 is appropriate.

Unlike thrust to weight ratio, the vehicle's I_{sp} has significant impact on the overall propellant mass fraction. To explore this further, trajectories were simulated for vehicles with specific impulses from 250 to 1000 sec. The range is expanded beyond the current technological limits to include hypothetical engines such as nuclear thermal rockets. The results are shown in Figure 11. As can be seen, increasing the specific impulse greatly impacts propellant mass fraction. Savings in propellant directly translate into more landed payload. For the 1000 sec I_{sp} case, the fully-propulsive trajectory from orbit satisfies the 0.5 W/cm^2 heat rate constraint with a lower PMF than that of the baseline vehicle flying the aeroassist reference trajectory. When mass sizing is performed for the vehicles in Figure 11, it is found that a vehicle which utilizes the fully-propulsive descent strategy from orbit with an I_{sp} of 645 sec has the same payload mass fraction of the equivalent aeroassist system.

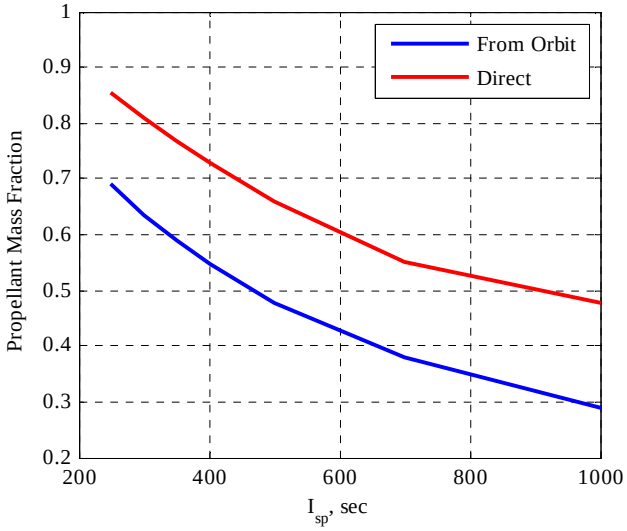

Figure 11 - Propellant Mass Fraction of the Baseline Vehicle with Various Specific Impulses

Mass Sizing

To study the impact of a fully-propulsive descent on mission capability, the payload mass fraction is calculated using the sizing methodology outlined earlier in this report. For comparison, the mass breakdowns of the baseline vehicle for the reference trajectory from orbit as well as the fully-propulsive descent with a heating rate constraint of 0.5 W/cm^2 are provided in Table 7. As expected, the fully-propulsive descent system sees a significant increase in needed propellant. The added propellant requires larger propellant tanks resulting in growth of the propulsion system mass. In this case, the mass benefit of eliminating the heatshield is overshadowed by the increase in propellant and

propulsion system mass, resulting in a drastically lower payload mass.

Table 7 - Mass Breakdown of the Baseline Vehicle for the From-Orbit Case

Subsystem	Reference Trajectory	Fully Propulsive Descent
	% of Initial Mass	
TPS	5.01	--
Structure	8.74	8.12
Propulsion System	6.33	10.04
Margin	10.48	9.74
Propellant	31.85	58.78
Payload	33.21	8.74

To further examine the sensitivity to the heat rate constraint, a series of cases were simulated. These cases included heat rate constraints ranging from 0.1 to 10 W/cm^2 and initial masses spanning 20 to 100 mT. Note that the cases with heat rate constraints greater than 1 W/cm^2 would need some form of TPS. In these cases, the use of propulsion during the descent would reduce the TPS requirements. The results of this study are presented in Figure 12 for the from-orbit cases and in Figure 13 for the direct entry cases. As seen in the figures, the payload mass fraction increases as the heat rate constraint increases. This is expected as a higher heat rate constraint allows for more deceleration due to drag and less propellant use throughout the trajectory. Figure 12 shows the extreme of this trend as the trajectories require no mid-trajectory burn to adhere to the heat rate constraint. This is shown as the lines for the 5, 7, and 10 W/cm^2 contours merge as the initial mass decreases.

Beyond the sensitivity to the heat rate constraint, Figures 12 and 13 show the feasibility limits of the current fully-propulsive descent architecture. Cases are deemed infeasible if the mass sizing algorithm assigns a negative payload mass fraction. In the scope of the study presented here, the from-orbit cases become infeasible for low initial masses (less than 50 mT) at very low heat rate constraints (0.1 – 0.25 W/cm^2). The direct entry cases are considerably more difficult and therefore result in many more failed cases. As seen in Figure 13, all cases with heat rate constraints less than 3 W/cm^2 are infeasible. By comparing Figures 12 and 13, it can be seen that a direct entry's payload mass fraction is approximately 30% less than a corresponding case from orbit for the baseline vehicle.

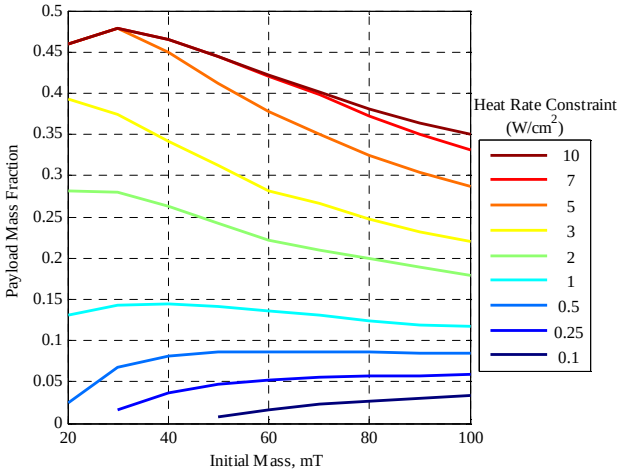

Figure 12 - Payload Mass Fraction for From-Orbit Fully-Propulsive Descent Cases

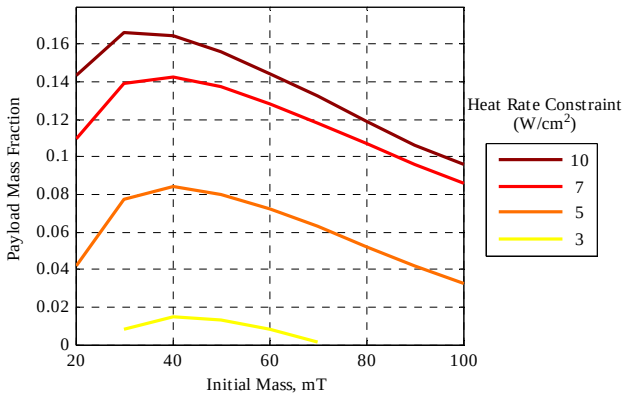

Figure 13 - Payload Mass Fraction for Direct Entry Fully-Propulsive Descent Cases

Mission Impact

Introduction of the fully-propulsive descent can significantly impact the dynamics and requirements of the EDL segment from a complexity, reliability, and mission architecture perspective.

Complexity—To analyze the effect of a fully-propulsive descent on the complexity of a mission, it is appropriate to analyze both hardware and operations. As offered in this study, a fully-propulsive descent may be used to avoid harsh heating environments usually encountered in atmospheric transit. In this light, the difficulty of developing and employing an enhanced propulsion system is being traded for that of TPS. The performance of the propulsion system greatly impacts the feasibility of the proposed EDL sequence. The specific impulse of 350 sec assumed in this study is widely accepted for LOX/CH_4 engines, and the thrust assumed for the baseline vehicle is approximately 700 kN (less than half of the thrust produced from one of the Space Shuttle's main engines). Throttling authority allows

for added control of the vehicle and enables the heat rate limited trajectories which allow elimination of the TPS. However, throttling of high-performance rocket engines is not easily achieved. The continuous throttling ability assumed in this study would likely be implemented as a series of discrete throttle settings at a small cost to performance.

Other concerns of the fully-propulsive descent sequence include thrusting into a hypersonic flow. Research focused on supersonic retropropulsion has examined thrusting into flows with Mach numbers up to 6 [20]; however, thrusting into flows with Mach numbers of up to 25 occurred in this study.

The difficulties of a fully-propulsive descent must be compared against those of a more conventional EDL sequence which relies on aeroassist strategies. One driver of complexity in an aeroassist trajectory is the reconfiguration of the vehicle during descent. These events often include the separation of the heatshield and backshell, deployment of a parachute or IAD, possible banking maneuvers for lifting trajectories, the use of novel aeroshell geometries for improved aerodynamic control authority, and a terminal thrusting maneuver. During an aeroassist trajectory, certain flight conditions must be met in order to successfully complete each of these events. For instance, a parachute or IAD must be deployed in a specific Mach and altitude envelop. These requirements are not present for a fully-propulsive descent.

Another source of complexity for an aeroassist trajectory is the development of the vehicle's TPS. This issue becomes increasingly difficult as the vehicle grows in size. Growth of the vehicle leads to paneling or tiling of the TPS material. Due to the limits in the size of individual panels or tiles, the quantity of the pieces needed to properly protect the vehicle increases as well as the number of seams between those pieces. This leads to increased risk and complexity as the vehicle becomes larger.

Reliability—In much the same way as complexity, reliability of a fully-propulsive descent can be compared against aeroassist EDL sequences. Of major concern would be the ability to initiate a large rocket engine after being dormant for a six to nine month transit period. However, this issue is present for many robotic deep space missions and is solved by focusing on engine reliability.

An increase in reliability of the fully-propulsive descent can also be realized if a divert capability is included in the EDL sequence. Divert maneuvers could be used during EDL to increase landing reliability by providing the ability to reach multiple landing sites. Diverting requires propulsive maneuvers at the end of a trajectory. For the case of an aeroassit trajectory, a divert maneuver must begin after parachute or IAD separation [25]. For a fully-propulsive descent, the divert maneuver may start at any point in the trajectory. This would increase the possible landing area thereby increasing the number of landing sites available or the range of abort-to-the-surface options.

Mission Architecture—Implementing a fully-propulsive descent during the EDL segment of a mission will impact the overall mission architecture. From the above analysis, a heat-rate limited direct entry requires a large propellant mass fraction which significantly decreases or eliminates the payload delivered to the Mars surface. As shown in this investigation, fully-propulsive descents are best implemented from orbit. Once entry-from-orbit is selected, an appropriate method for orbit insertion must be determined. Due to the availability of a capable propulsion system, propulsive insertion may be possible. However, the burn to transfer the vehicle from the hyperbolic approach to the 400 km altitude circular orbit requires approximately 2.5 km/sec of ΔV. This results in a propellant mass fraction on the order of 50% for the orbit insertion burn. If all of the needed propellant is to be transported from Earth, the baseline vehicle with a mass of 60 mT in Mars orbit grows to over 350 mT at Earth departure. However, an in-situ supplied propellant depot in Mars orbit would allow a mission architecture in which the spacecraft refuels after insertion into Mars orbit [26]. In this approach, the vehicle would travel to Mars, use its Earth-based propellant to insert into Mars orbit, and then refill its tanks at the Mars propellant depot before initiating the fully-propulsive descent to the Mars surface.

Another orbit insertion option at Mars is aerocapture. This maneuver is suggested by Christian et al. [18]. A similar orbit insertion maneuver is possible for the current study. If paired with refueling at Mars, the fully-propulsive descent allows for a much lower mass aerocapture system (a baseline vehicle with a mass of approximately 30 mT). After the aerocapture maneuver, the vehicle can rendezvous with the propellant depot and take on the fuel needed for the fully-propulsive descent.

Finally, the lack of dependency on aerodynamic forces places less of a demand on shaping the aeroshell for those purposes. Although not examined in this study, a fully-propulsive descent allows for more flexibility in the shape of the vehicle. This in turn lets the vehicle be designed for surface operations instead of survival of EDL. As a result, the vehicle can be designed with a larger habitable volume, easier entry and egress systems, or compatibility with prepositioned surface assets. The increased functionality of the vehicle may lead to a simpler and more productive surface operations phase.

4. CONCLUSIONS

This study has explored the use of propulsion during the EDL sequence at Mars for high-payload missions. The study focused on replacing the conventional aeroassist EDL

strategies with one that relies solely on propulsion. For the study, trajectory simulation and mass sizing were performed to analyze the feasibility of a fully-propulsive descent. Trajectories guided along a heat rate constraint were presented in an effort to avoid the use of TPS. The results show that the fully-propulsive descent strategy is best implemented after the vehicle has been inserted into Mars orbit. When performed in this manner, the proposed EDL strategy is able to deliver surface payloads of 0.5 – 8.4 mT for vehicles with initial masses of 20 – 100 mT. The payload mass fractions of the cases presented in this study range from 2.5 – 8.7%. These values are much lower than the values suggested by other Mars mission studies. However, the performance of the presented architecture strongly depends on the propulsion system's performance. The analysis showed that fully-propulsive EDL strategies become attractive for vehicles with specific impulses over 650 sec. Future work should include further exploration of control algorithms for the powered descent portion of trajectories, a quantitative analysis of divert capabilities, impact of decreases in aerodynamic drag during propulsive maneuvers, and an integration of the fully-propulsive descent strategy into a Mars reference mission.

To enable high payload missions to Mars, conventional aeroassist strategies require further technology development in multiple areas such as TPS, inflatable aerodynamic decelerators, supersonic parachutes, and aeroshell configurations; whereas, a fully-propulsive descent strategy would require technology advancements in high-thrust, high-I_{sp} propulsion systems.

ACKNOWLEDGEMENTS

The authors would like to thank the students and faculty of the Space Systems Design Laboratory at the Georgia Institute of Technology, especially Ian Clark, Michael Grant, Ashley Korzun, and Bradley Steinfeldt.

REFERENCES

[1] R.D. Braun and R.M. Manning, "Mars Entry, Descent, and Landing Challenges," Journal of Spacecraft and Rockets, Vol. 44, No. 2, 310-323, March-April 2007.

[2] R. Prakash, et al. "Mars Science Laboratory Entry, Descent, and Landing System Overview," 2008 IEEE Aerospace Conference Proceedings, March 1-8, 2008.

[3] "Vision for Space Exploration," National Aeronautics and Space Administration, NASA NP-2004-01-334-HQ, February 2004.

[4] B.G. Drake (ed.), "Reference Mission Version 3.0 Addendum to the Human Exploration of Mars: The Reference Mission of the NASA Mars Exploration Study Team," NASA/SP-6107-ADD, June 1998.

[5] D.C. Cheatham and F.V. Bennett, "Apollo Lunar Module Landing Strategy," Apollo Lunar Landing Symposium, June 1966.

[6] C.G. Cooley and J.G. Lewis, "Viking Lander System Primary Mission Performance Report," NASA CR-145148, April 1977.

[7] R.N. Ingoldby, et al., "Entry Data Analysis for Viking Landers 1 and 2," NASA CR-159388, November 1976.

[8] D.C. Morrisey, "Historical Perspective: Viking Mars Lander Propulsion," Journal of Propulsion and Power, Vol. 8, No. 2, 320-331, March-April 1992.

[9] D. A. Spencer, et al., "Mars Pathfinder Entry, Descent, and Landing Reconstruction," Journal of Spacecraft and Rockets, Vol. 36, No. 3, 357-366, May-June 1999.

[10] D.K. McGrath and C.E. Carr II, "Mars Pathfinder Retrograde Rocket Development," 34th AIAA/ASME/SAE/ASEE Joint Propulsion Conference and Exhibit, Cleveland, Ohio, July 13-15, 1998.

[11] P.N. Desai and P.C. Knocke, "Mars Exploration Rovers Entry, Descent, and Landing Trajectory Analysis," AIAA/AAS Astrodynamics Specialist Conference and Exhibit, Providence, Rhode Island, August 16-19, 2004.

[12] C.A. Moore and C. Guernsey, "Development and Qualification of the Rocket-Assisted Deceleration (RAD) and Transverse Impulse Rocket System (TIRS) Motors for the Mars Exploration Rover (MER)," 52nd Joint Army-Navy-NASA-Air Force (JANNAF) Propulsion Meeting, Las Vegas, Nevada, May 10-13, 2004.

[13] M.R. Grover III, B.D. Cichy, and P.N. Desai, "Overview of Phoenix Entry, Descent, and Landing System Architecture," AIAA Guidance, Navigation, and Control Conference, Honolulu, Hawaii, August 2008.

[14] J.L. Prince, et al., "Mars Phoenix Entry, Descent, and Landing Simulation Design and Modeling Analysis," AIAA Guidance, Navigation, and Control Conference, Honolulu, Hawaii, August 2008.

[15] B. Goldstein and R. Shotwell, "Phoenix - The First Mars Scout Mission (A Mid-Term Report)," Acta Astronautica 57, 121-134, July-October 2005.

[16] R.W. Powell, S.A. Striepe, P.N. Desai, and R.D. Braun, "Program to Optimize Simulated Trajectories (POST), Utilization Manual," Version 5.0, September 1996.

[17] B.A. Steinfeldt, M.J. Grant, D.M. Matz, R.D. Braun, and G.H. Barton, "Guidance, Navigation and Control Technology System Trades for Mars Pinpoint Landing," 2008 AIAA Atmospheric Flight Mechanics Conference, August 2008.

[18] J. Christian, et al., "Extension of Traditional Entry, Descent, and Landing Technologies for Human Mars Exploration," Journal of Spacecraft and Rockets, Vol. 45, No.1, 130-141, January-February 2008.

[19] I.A. Klepikov, I.A. Katorgin, and V.K. Chvanov, "The New Generation of Rocket Engines, Operating by Ecologically Save Propellant 'Liquid Oxygen and Liquefied Natural Gas (Methane)'," Acta Astronautica, Vol. 41, No. 4-10, 209-217, 1997.

[20] A.M. Korzun, J.R. Cruz, and R.D. Braun, "A Survey of Supersonic Retropropulsion Technology for Mars Entry, Descent, and Landing," IEEE Aerospace Conference Proceedings, Big Sky, Montana, March 1-8, 2008.

[21] R.W. Humble, G.N. Henry, and W.J. Larson, "Space Propulsion Analysis and Design," McGraw-Hill Companies, New York, 1995.

[22] M.E. Tauber and K. Sutton, "Stagnation-Point Radiative Heating Relations for Earth and Mars Entries," Journal of Spacecraft and Rockets, Vol. 28, No. 1, 40-42, January-February 1991.

[23] B. Laub and R. Venkatapathy, "Thermal Protection System Technology and Facility Needs for Demanding Future Planetary Missions," International Workshop on Planetary Probe Atmospheric Entry and Descent Trajectory Analysis and Science, Lisbon, Portugal, October 6-9, 2003.

[24] P. Knowles, Design of Structural Steelwork, London: Taylor & Francis, 1987.

[25] M.J. Grant and R.D. Braun, "Smart Divert: A New Entry, Descent, and Landing Architecture," 47th AIAA Aerospace Sciences Meeting Proceedings, January 5-8, 2009.

[26] J. Powell, G. Maise, and J. Paniagua, "A Self-Sustaining Earth-Mars Architecture Utilizing Martian Colonies Based on the North Polar Cap," 2001 IEEE Aerospace Conference Proceedings, March 10-17, 2001.

BIOGRAPHY

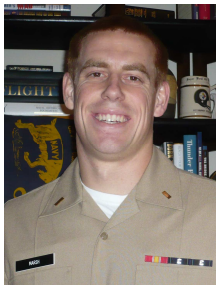

Christopher L. Marsh *is an Ensign in the United States Navy. He is currently an aerospace engineering graduate student at the Georgia Institute of Technology in the Space Systems Design Laboratory. His research focuses on the use of propulsion during EDL sequences. He has previously interned at Los Alamos National Laboratory and Johnson Space Center. Chris has a B.S. in Systems Engineering from the United States Naval Academy.*

Robert D. Braun *is the David and Andrew Lewis Associate Professor of Space Technology in the Daniel Guggenheim School of Aerospace Engineering at the Georgia Institute of Technology. As Director of Georgia Tech's Space Systems Design Laboratory, he leads a research program focused on the design of advanced flight systems and technologies for planetary exploration. He is responsible for undergraduate and graduate level instruction in the areas of space systems design, astrodynamics, and planetary entry. Prior to coming to Georgia Tech, he served on the technical staff of the NASA Langley Research Center for sixteen years, where he contributed to the design, development, test, and operation of several robotic space flight systems. He has worked extensively in the areas of entry system design, planetary atmospheric flight, and mission architecture development. Dr. Braun is an AIAA Fellow and the principal author or co-author of over 150 technical publications in the fields of planetary exploration, atmospheric entry, multidisciplinary design optimization, and systems engineering. He has a B.S. in Aerospace Engineering from Penn State University, a M.S. in Astronautics from George Washington University, and a Ph.D. in Aeronautics and Astronautics from Stanford University.*